Incorporating LWIR Data into Multi-Frame Blind Deconvolution of Visible Imagery

Michael Werth, Brandoch Calef, Daniel Thompson
The Boeing Company

Lisa Thompson
Air Force Research Laboratory

ABSTRACT

The 3.6m telescope at the Air Force Maui Optical and Supercomputing (AMOS) site is able to send light to a Long Wave Infrared (LWIR) sensor and a visible imaging sensor for simultaneous recording in different wavebands. LWIR images suffer less from atmospheric blurring than visible images, therefore it should be possible to use LWIR information to provide a priori information to a Multi-Frame Blind Deconvolution (MFBD) algorithm that reconstructs visible images. This would result in better image reconstructions that are produced in less time. We describe techniques for fusing LWIR and visible data for MFBD processing, and we apply these techniques to a number of Low Earth Orbit (LEO) satellite collections. Measured improvements in processing time and reconstructed image resolution are presented.

1. INTRODUCTION

Ground-based observations of satellites in Low Earth Orbit (LEO) are blurred by atmospheric turbulence. This blur is difficult to remove due to the random and frequently-changing nature of the atmospheric blurring function. Multi-Frame Blind Deconvolution (MFBD) is a family of speckle imaging algorithms that attempt to estimate a pristine image of an object image from an ensemble of atmospherically blurred short exposure images without prior knowledge of the Point Spread Function (PSF) [1]. These algorithms frequently differ in their initial assumptions, choice of numerical estimator, and approach to regularization, but they all assume that the object has a region of finite support. The size and shape of the support region must be estimated from the data, and the ability of support estimation algorithms to produce a support region that closely approximates the final recovered image can have a significant impact on image quality and processing time.

Images recorded in a longer wavelength experience less atmospheric blurring. This advantage is leveraged by Wavelength Diversity algorithms that attempt to perform simultaneous MFBD in multiple wavebands, but these algorithms impose a number of engineering challenges [2,3]. Without fully committing to a Wavelength Diversity algorithm, one can still leverage superior LWIR initial object shape information by generating an estimate of the object support from LWIR data and using it during MFBD processing of visible data. This technique is less sensitive to optical path difference variations between wavebands, differences in timing between waveband frame readouts, and differences in sensor noise statistics. This paper demonstrates LWIR object support estimation and applies it to the Physically Constrained Iterative Deconvolution (PCID) MFBD algorithm [4,5] for several satellite collections.

In Section 2, techniques for generating an object support region for visible and LWIR imagery are described. In Section 3, benchmarks and image quality results are shown for several LEO satellites that are MFBD processed with and without LWIR support estimation. Section 4 contains conclusions and potential improvements.

2. SUPPORT ESTIMATION

A finite support is commonly used as a formulating assumption in many blind deconvolution techniques [6]. A well-defined support has an additional practical advantage in that an optimal reconstruction is produced in less time, as pixels outside of the support region can be ignored. The PCID algorithm estimates the object support by thresholding the mean of several centered measurement frames [4]. However, if the long exposure PSF diameter is greater than the diameter of the true object then the estimated support will be much larger than the pristine object's size. This introduces noise-only regions of the image into the estimation process, degrading reconstructed image

quality and increasing processing time. Other causes of a misestimated support can include poor SNR and sensor miscalibration. Fig. 1 shows an example of a well-defined object support, made possible with a functioning Adaptive Optics (AO) system removing much of the atmospheric blur. Fig. 2 shows an example of a poorly-defined object support due to strong turbulence and poor SNR.

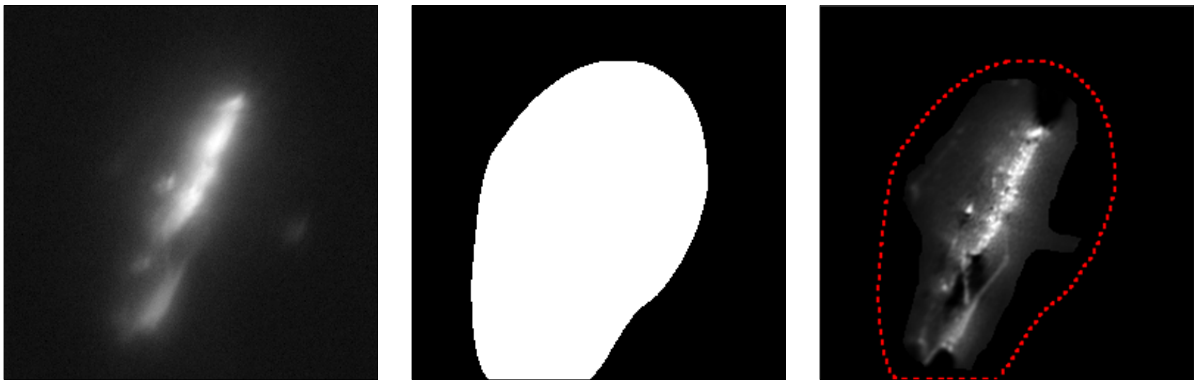

(a) (b) (c)

Fig. 1. (a) Raw HST image with AO compensation,
(b) PCID-generated support for HST image with AO compensation, and
(c) PCID-generated support with overlaid final reconstruction of HST

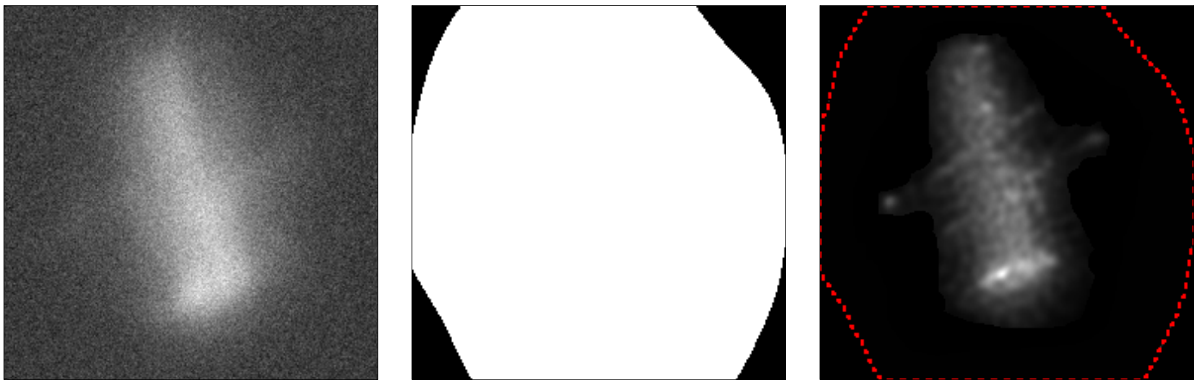

(a) (b) (c)

Fig. 2. (a) Raw HST image without AO compensation,
(b) PCID-generated support of HST without AO compensation, and
(c) PCID-generated support with overlaid final reconstruction of HST

LWIR images have unique advantages when it comes to support estimation. Fried's parameter r_0 increases with wavelength, corresponding with a smaller PSF diameter [7]. This waveband is also less sensitive to poor target illumination. We use a straightforward procedure for estimating the object support from LWIR images. Otsu's thresholding method [8] is combined with a 5x5 Gaussian blurring kernel and dilation in order to produce a mask of the object in LWIR. The mask is translated to the center of the image array, rotated to the same orientation as the visible image, and resized to have a field of view per pixel that is 10% greater than the visible image in order to minimize the likelihood of real object features falling outside of the support. This process is shown in Fig. 3 using LWIR images that were recorded at the same time as the visible images that are shown in Fig. 2.

3. RESULTS

LWIR and visible datasets were collected simultaneously for ten LEO satellites with varying atmospheric conditions. PCID reconstructions were generated for each visible dataset using object support regions generated

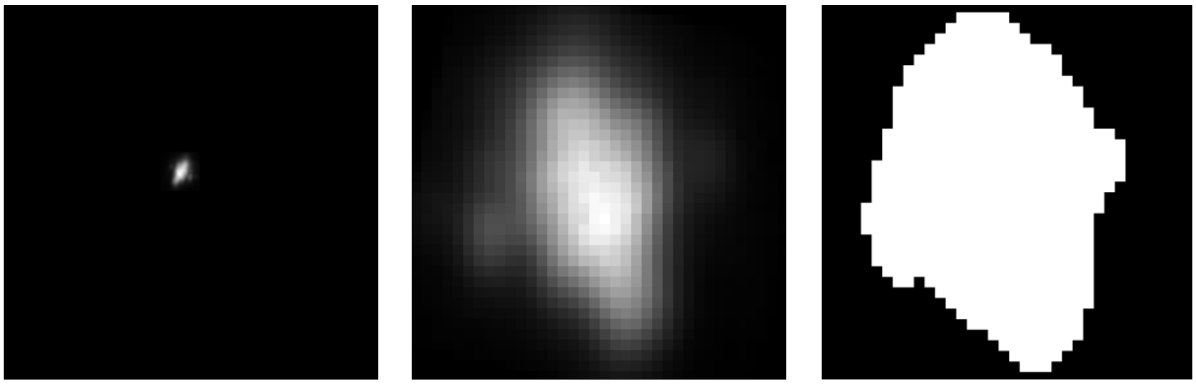

(a) (b) (c)

Fig. 3. (a) LWIR image of HST,
(b) LWIR image converted to Visible orientation and field of view, and
(c) Object support generated from LWIR image

from the visible data. The same collections underwent PCID processing a second time with an automatically generated object support region from LWIR data. This procedure was repeated three times per collection in order to collect benchmarks of average processing time with and without the object support generated from LWIR data. In every case, using LWIR to generate the object support improved processing time, sometimes reducing processing time by over 50%. Images that were produced with AO compensation resulted in well-defined object support regions from visible data, and in these cases there was relatively little improvement when the LWIR-based support was used. Values of the percentage change in processing time, $P\Delta t$, for data collections with an AO system is shown in Table 1. Values of $P\Delta t$ for collections without AO system are shown in Table 2.

In order to ascertain whether there was a change in image quality, two image quality metrics were used. The first is a blind full-frame metric referred to as Laplacian of Gaussian (LoG), which is the sum of the modulus square of the pixel values of the image after it has been convolved with a Laplacian of Gaussian filter [9]. The second is a blind local metric referred to as the Mean Measured Line Spread Function (MMLSF) measure; this metric captures the mean full width at half maximum of the line spread function from a number of the object's space-neighboring edges [10]. Percentage change values for each of these metrics, $P\Delta LoG$ and $P\Delta \mathrm{MM}LSF$, are shown in Table 1 for data collected without AO compensation and in Table 2 for data that was recorded with AO compensation.

Table 1: The percentage change in processing time and image quality metrics when the LWIR object support algorithm was used for satellite collections without AO compensation. LoG and LSF metrics were defined in Section 3. Positive values denote an improvement when the LWIR object support was used.

LEO Satellite name	$P\Delta t$	$P\Delta LoG$	$P\Delta \mathrm{MM}LSF$
ASTEX 1	18.7%	10%	12%
Fermi Gamma-ray Space Telescope (GLAST)	19.7%	50%	19%
Hubble Space Telescope (HST) (Night 1)	39.9%	20%	15%
Iridium 82	14.4%	40%	9%

Table 2: The percentage change in processing time and image quality metrics when the LWIR object support algorithm was used for satellite collections with AO compensation. LoG and LSF metrics were defined in Section 3. Positive values denote an improvement when the LWIR object support was used.

LEO Satellite name	$P\Delta t$	$P\Delta LoG$	$P\Delta \mathrm{MM}LSF$
Delta 1 Rocket Body	12.8%	10%	7%
Fermi Gamma-ray Space Telescope (GLAST)	4.3%	10%	6%
Hubble Space Telescope (HST) (Night 2)	21.4%	20%	-4%
Hubble Space Telescope (HST) (Night 3)	41.4%	30%	1%

Fig. 4 shows a GLAST collection without AO compensation. The seeing was relatively good during this collection, as can be seen from Fig. 4a. Despite that, the LWIR object support still more accurately represented the pristine object than the visible image. PCID processing was about 20% faster when the object support was generated from LWIR data, and there were also improvements in image quality. Comparing Fig. 4a to Fig. 4b by eye, the noisy pixels around the central body are a little brighter when the LWIR support is not used. Equivalent levels of contrast were applied to Fig. 4c and Fig. 4d.

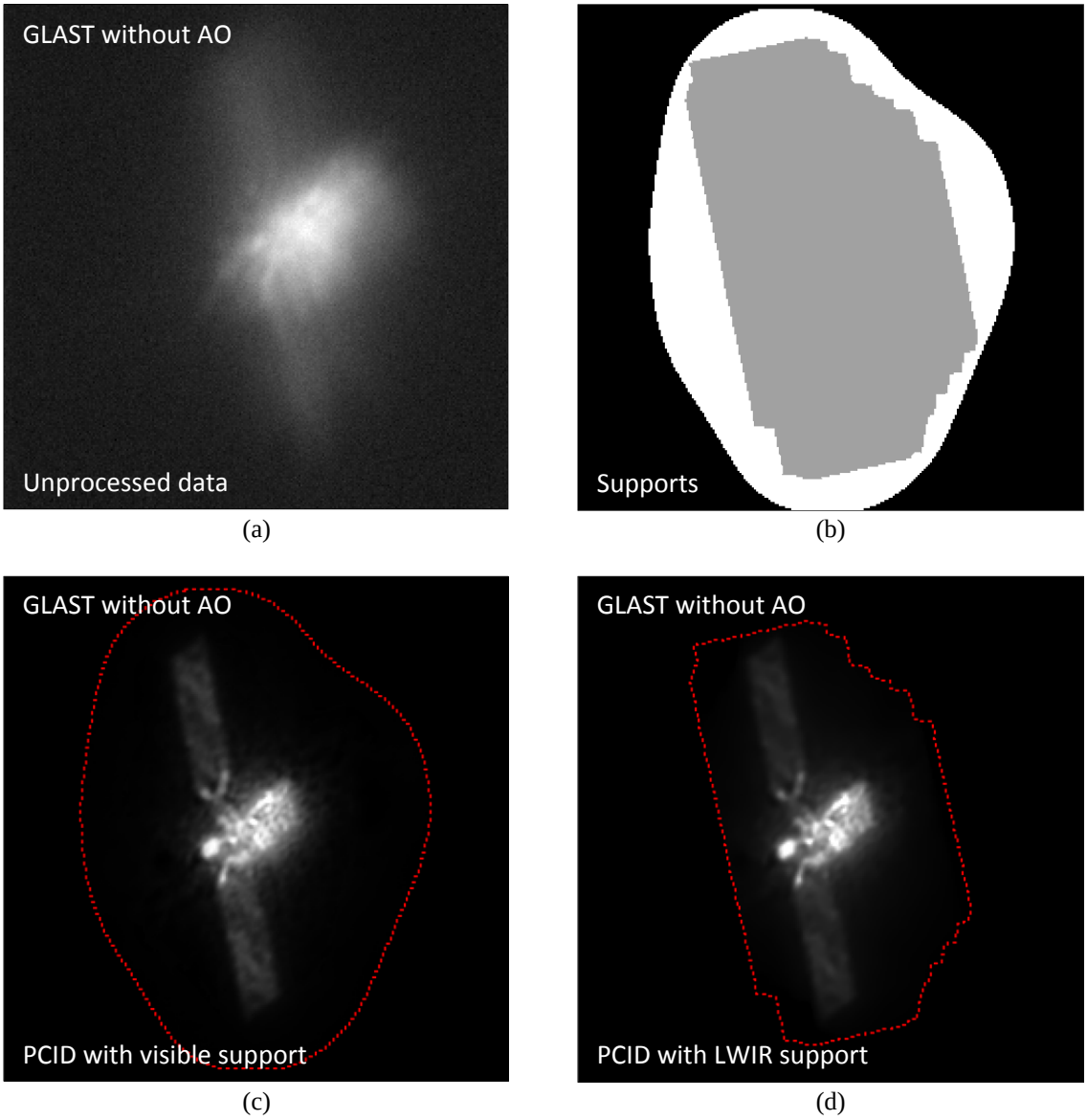

Fig. 4. (a) Raw visible collection of GLAST satellite without AO compensation,
(b) Object support generated from Visible (white) and LWIR (grey),
(c) PCID-processed GLAST satellite with object support calculated from visible data, and
(d) PCID-processed GLAST satellite with object support calculated from LWIR data.

Fig. 5 shows a collection of ASTEX1 without AO compensation. The seeing was particularly bad during this pass, and as a result the visible-generated object support is particularly large. When using the much smaller LWIR-generated object support there is a significant improvement in processing time and a measured improvement in image quality. Equivalent levels of contrast were applied to Fig. 5c and Fig. 5d.

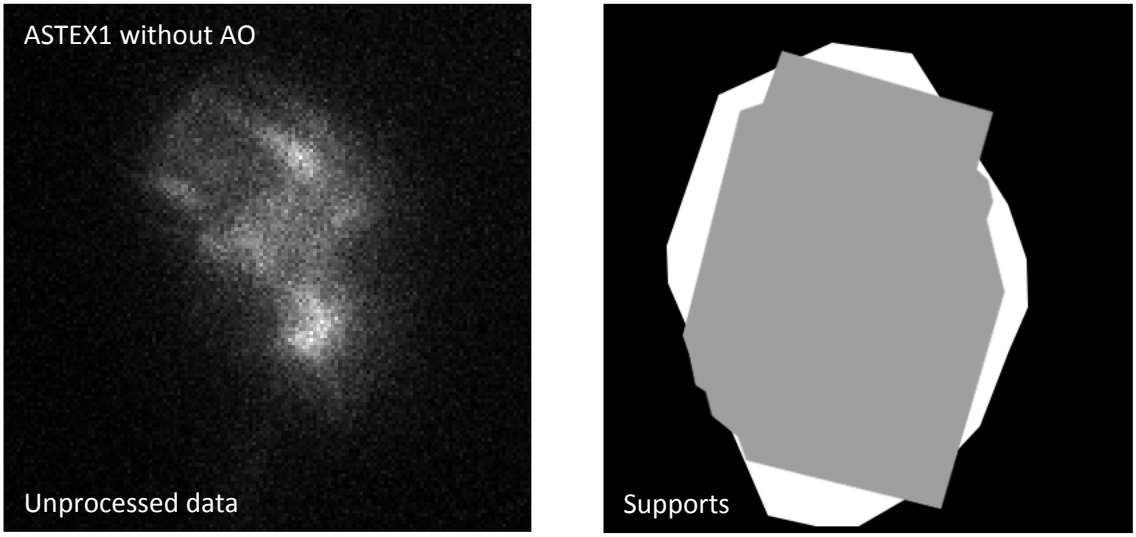

(a)

(b)

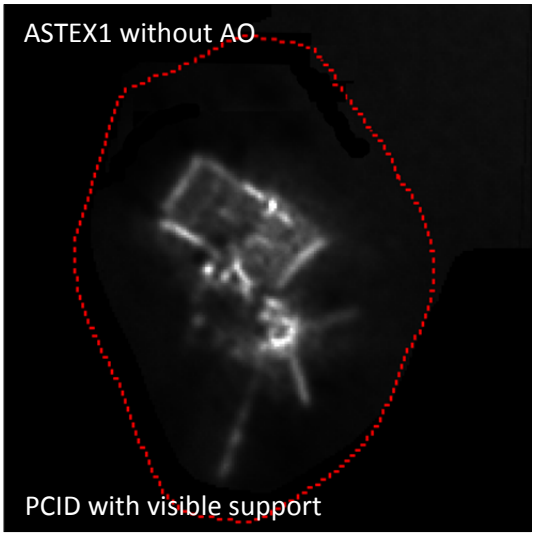

(c)

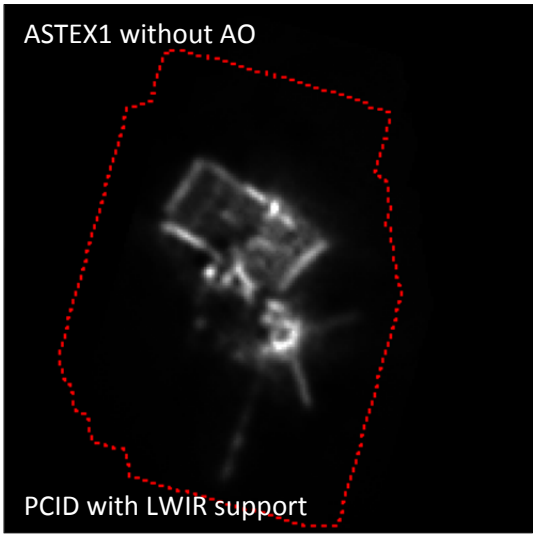

(d)

Fig. 5. (a) Raw visible collection of GLAST satellite with AO compensation,
(b) Object support generated from Visible (white) and LWIR (grey),
(c) PCID-processed GLAST satellite with object support calculated from visible data, and
(d) PCID-processed GLAST satellite with object support calculated from LWIR data.

Fig. 6 shows a GLAST collection with AO compensation. The visible object support roughly approximates the LWIR object support, as seen in Fig. 6b. This leaves relatively little room for improvement; Table 1 confirms only a small improvement in processing time and no significant change in image quality. Equivalent levels of contrast were applied to Fig. 6c and Fig. 6d.

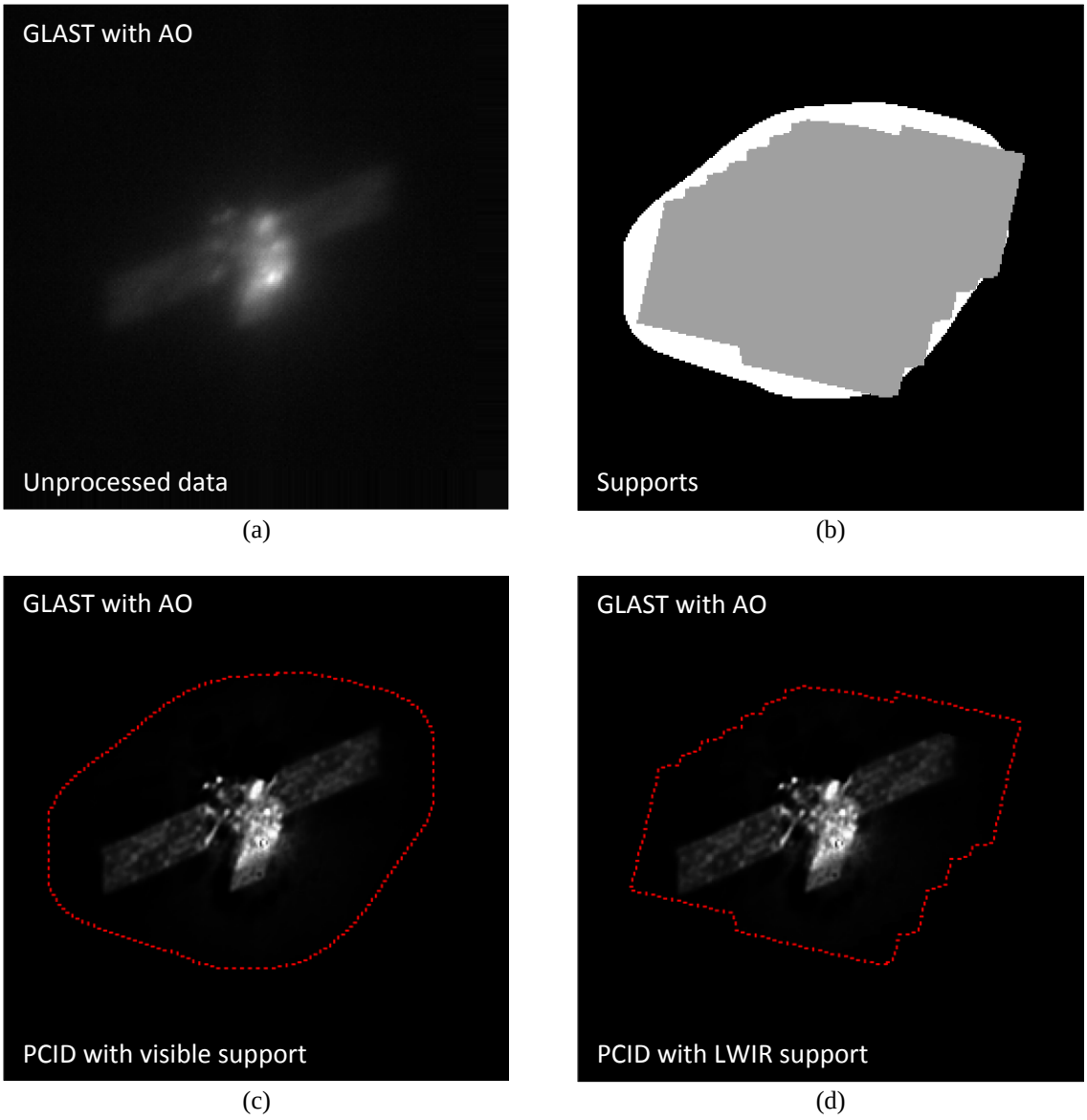

Fig. 6. (a) Raw visible collection of GLAST satellite with AO compensation,
(b) Object support generated from Visible (white) and LWIR (grey),
(c) PCID-processed GLAST satellite with object support calculated from visible data, and
(d) PCID-processed GLAST satellite with object support calculated from LWIR data.

Fig. 7 shows an HST collection with AO compensation, designated as "Night 2" in Table 2. The visible object support roughly approximates the LWIR object support, as seen in Fig. 7b, and there is no significant change in image quality. However, despite the LWIR support mask having a pixel area that is only 0.6% smaller than the visible support mask, the processing time decreased by over 20%. This is an unexpected result. The reason for this is unclear at this time, but it could be as simple as the LWIR support keeping a larger fraction of speckle pixels and a smaller fraction of background pixels than the visible support.

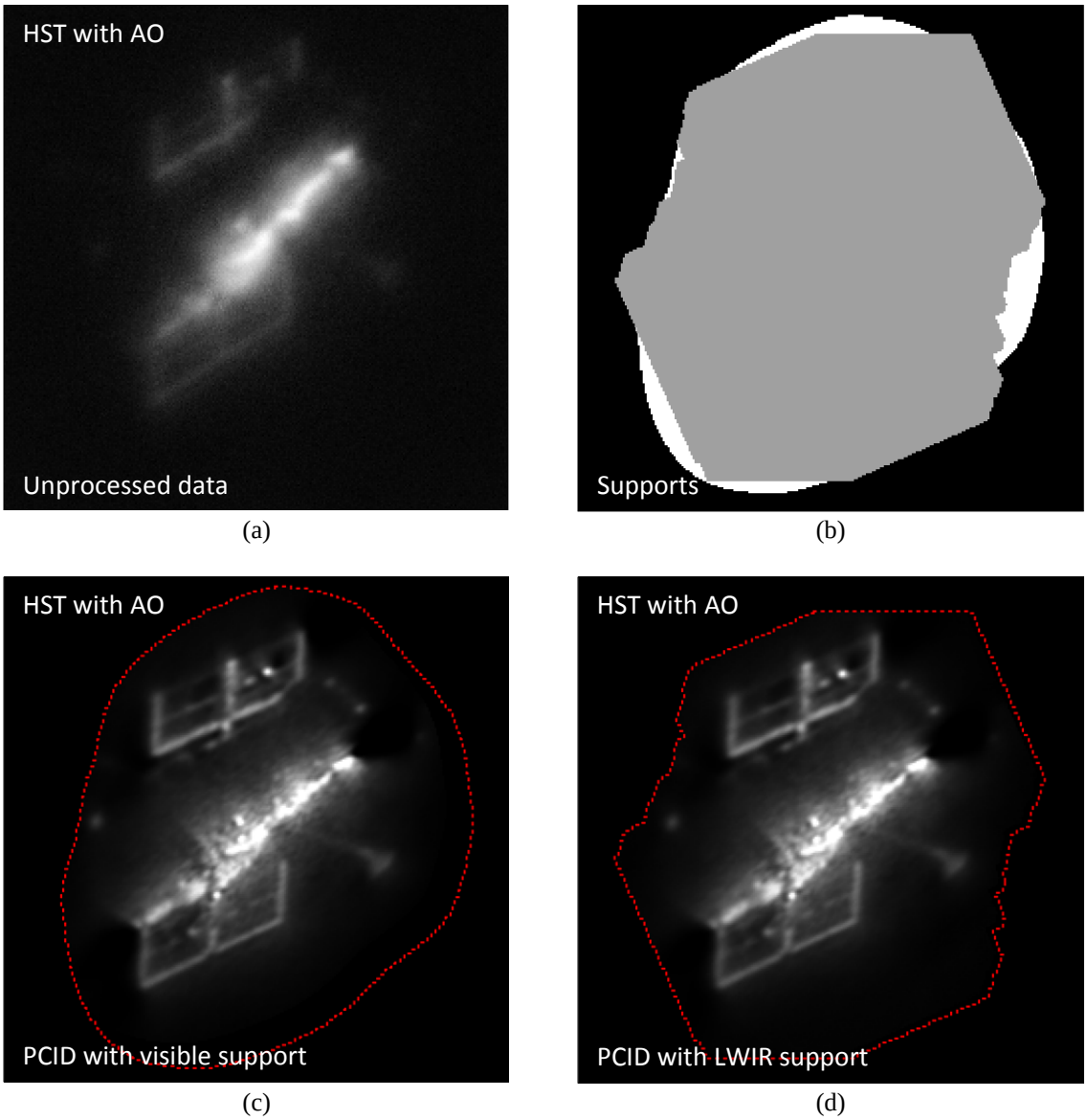

Fig. 7. (a) Raw visible collection of HST satellite with AO compensation,
(b) Object support generated from Visible (white) and LWIR (grey),
(c) PCID-processed HST satellite with object support calculated from visible data, and
(d) PCID-processed HST satellite with object support calculated from LWIR data.

Fig. 8 shows an interesting case where the LWIR object support cut off several of the Hubble Space Telescope's features. These images correspond to the "HST Night 3" entry in Table 2. Several recovered frames from this collection have the lower left solar panel, right-side antenna, or upper door clipped by the LWIR-generated object support. It is unclear at this time why the LWIR support was so much smaller than the visible support.

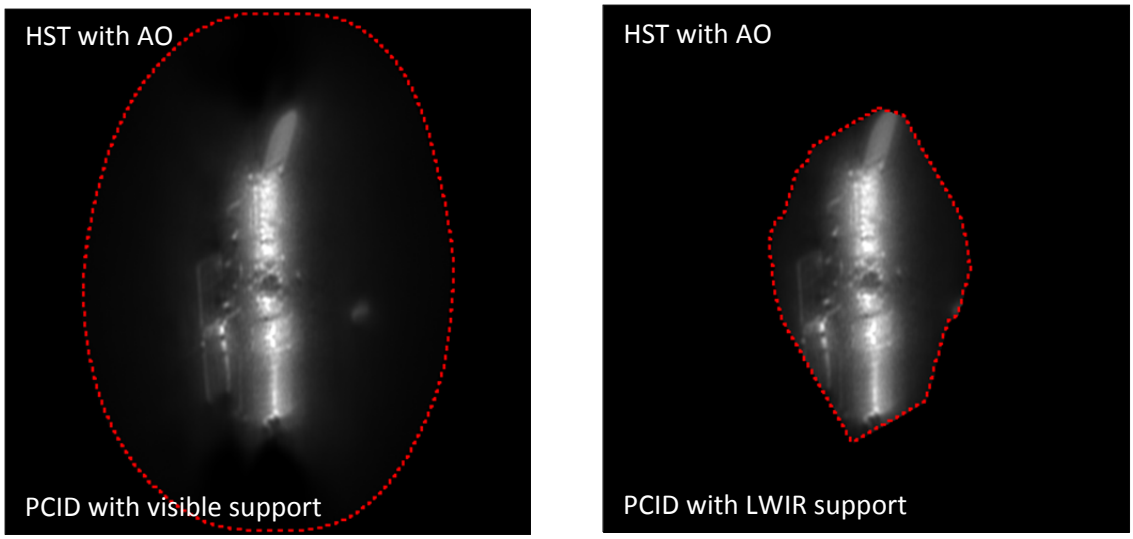

(a) (b)

Fig. 8. (a) HST processed with visible object support highlighted in grey and (b) processed with LWIR object support highlighted in grey, showing evidence that several features have been clipped by the LWIR object support, including the door at the top, the solar panel in the bottom left, and the antenna on the right.

4. CONCLUSIONS

We have described a method for estimating an initial object support region using simultaneously collected LWIR images. Atmospheric turbulence in this waveband has a much weaker blurring effect than in visible wavebands, and this often results in a support region that more closely surrounds the true object than an estimated support that relies on visible imagery. Using ten LEO satellite collections, it was shown that this technique significantly improves processing time and marginally improves image quality.

Some anomalous results were found during testing. Processing AO-compensated HST data with an LWIR support appeared to significantly reduce processing time despite not significantly effecting image quality and despite the LWIR object support region being only 0.6% smaller than the visible object support region. A different HST collection had features of the object being clipped off by the LWIR object support.

This algorithm could undergo a number of improvements. In order to minimize the likelihood of real visible object features being cut off by those features not appearing in LWIR wavebands while maintaining an optimally tight support, an algorithm that blends the visible and LWIR data prior to creating the object support could be developed. Anti-aliasing the LWIR-based support could improve the rate at which noise-only pixels are removed while simultaneously reducing the chance of object feature clipping. It might also be interesting to see how MFBD processing is effected by using anti-aliased LWIR data as an initial object estimate.

5. ACKNOWLEDGEMENTS

The Air Force Research Laboratory and the Air Force Office of Scientific Research provide the funding that makes this kind of work possible, and the authors would like to thank these organizations for their continued support.

6. REFERENCES

1 H.W. Babcock, "The Possibility of Compensating Astronomical Seeing," Pub. Of the Astron. Soc. Of the Pacific, v. 65, n. 386 (1953).

2 Ingleby, H.R. and McGaughey, D.R. "Experimental results of parallel multiframe blind deconvolution using wavelength diversity." Proc. SPIE 5578, Photonics North 2004: Photonic Applications (2004).

3 Burke, D., Devaney, N., Christou, J., Hartung, M. "Application of wavelength diversity for astronomical adaptive optics imaging." Proc. SPIE 7736, Adaptive Optics Systems II (2010).

4 Matson, C.L., Beckner, C.C., Boreilli, K., Jeffries, S.M., Hege, E.K., Lloyd-Hart, M. *A fast and optimal multi-frame blind deconvolution algorithm for high-resolution ground-based imaging of space objects*." Applied Optics, 48, A75-A92 (2009).

5 Matson, C.L., Beckner, C.C., Borelli, K., Hoo, T.S., You, S., Calef, B., Murphy, M., Viloria, R., *PCID and ASPIRE 2.0 – the next generation AMOS image processing environment.* Proceedings of the 2007 AMOS Technical Conference (2007).

6 Lane, R.G. and Bates, R.H.T. "Automatic multidimensional deconvolution." J. Opt. Soc. Am. **A** 4, 180-188 (1987).

7 Fried, D. "Optical Resolution Through a Randomly Inhomogenous Medium for Very Long and Very Short Exposures." J. Opt. Soc. Am. 56, 1372-1379 (1966).

8 Otsu, N. "A Threshold Selection Method from Gray-Level Histograms." Systems, Man, and Cybernetics, IEEE Transactions, v. 9, n. 1 (1979).

9 Bos, J. and Roggemann, M. "Blind image quality metrics for optimal speckle image reconstruction in horizontal imaging scenarios." Opt. Eng. 51(10), 107003 (2012).

10 Werth, M. Calef, B., Thompson, D., Bos, J., Williams, St., Williams, Sk. "A New Performance Metric for Hybrid Adaptive Optics Systems." Proceedings of the 2014 IEEE Aerospace Conference (2014).